FEB 28 2005

REPORT DOCUMENTATION PAGE	Form Approved OMB No. 0704-0188

1. AGENCY USE ONLY *(Leave blank)*	2. REPORT DATE	3. REPORT TYPE AND DATES COVERED
	24.Feb.05	MAJOR REPORT

4. TITLE AND SUBTITLE
QUANTIFYING POLARIZED CLUTTER IN THE VISIBLE TO NEAR-INFRARED

5. FUNDING NUMBERS

6. AUTHOR(S)
MAJ SHELL JAMES R II

7. PERFORMING ORGANIZATION NAME(S) AND ADDRESS(ES)
ROCHESTER INSTITUTE OF TECHNOLOGY

8. PERFORMING ORGANIZATION REPORT NUMBER
CI04-972

9. SPONSORING/MONITORING AGENCY NAME(S) AND ADDRESS(ES)
THE DEPARTMENT OF THE AIR FORCE
AFIT/CIA, BLDG 125
2950 P STREET
WPAFB OH 45433

10. SPONSORING/MONITORING AGENCY REPORT NUMBER

11. SUPPLEMENTARY NOTES

12a. DISTRIBUTION AVAILABILITY STATEMENT
Unlimited distribution
In Accordance With AFI 35-205/AFIT Sup 1

12b. DISTRIBUTION CODE

13. ABSTRACT *(Maximum 200 words)*

DISTRIBUTION STATEMENT A
Approved for Public Release
Distribution Unlimited

14. SUBJECT TERMS

15. NUMBER OF PAGES
12

16. PRICE CODE

17. SECURITY CLASSIFICATION OF REPORT	18. SECURITY CLASSIFICATION OF THIS PAGE	19. SECURITY CLASSIFICATION OF ABSTRACT	20. LIMITATION OF ABSTRACT

Quantifying polarized clutter in the visible to near-infrared

James R. Shell, II[a] and John R. Schott[b]

[a]U.S. Air Force & Rochester Institute of Technology;
[b]Digital Imaging and Remote Sensing Laboratory
Chester F. Carlson Center for Imaging Science, Rochester Institute of Technology
54 Lomb Memorial Drive, Rochester, NY 14623

ABSTRACT

Polarization adds another dimension to the spatial intensity and spectral information typically acquired in remote sensing. Polarization imparted by surface reflections contains unique and discriminatory signatures which may augment spectral target-detection techniques. While efforts have been made toward quantifying the polarimetric bidirectional reflectance distribution function (BRDF) responsible for target material polarimetric signatures, little has been done toward developing a description of the polarized background or scene clutter. An approach is presented for measuring the polarimetric BRDF of background materials such as vegetation.

The governing equation for polarized radiance reaching a sensor aperture is first developed and serves as a basis for understanding outdoor polarimetric BRDF measurements, as well as polarimetric remote sensing. The polarimetric BRDF measurements are acquired through an imaging technique which enables derivation of the BRDF variability as a function of the ground separation distance (GSD). An image subtraction technique is used to minimize measurement errors resulting from the partially polarized downwelled sky radiance. Quantifying the GSD-dependent BRDF variability is critical for background materials which are typically spatially inhomogeneous. Preliminary results from employing the measurement technique are presented.

Keywords: Polarization, BRDF, clutter, target detection, multispectral

1. INTRODUCTION

Polarimetric remote sensing in the visible to near-infrared (VNIR), or in the spectral regime dominated by solar energy, has long been shown to offer advantages over intensity-only imaging.[1–4] Benefits such as improving man-made object detection are often touted, as well as possible improvements to spectral algorithms used for detection and identification.[5] However, virtually all efforts fail to cast polarimetric remote sensing within a cohesive framework in which *a priori* predictions of the target polarized radiance are made, as is done with spectral remote sensing techniques. There is also a need to accurately represent and model the polarized background or clutter environment. The ability to model target and background polarimetric signatures is a prerequisite for exploring the benefits polarization adds to spectral target detection and classification algorithms. Polarimetric signature models may then be implemented into radiometrically accurate synthetic image generation programs.

First, the bidirectional reflectance distribution function (BRDF) is introduced and the more general polarimetric BRDF, which quantifies polarized signatures. Next, the governing equation for polarized radiance reaching a sensor is developed. The equation highlights the role of the polarimetric BRDF, and also serves as a foundation for polarimetric remote sensing. The governing equation guides the implementation of the outdoor measurement technique for quantifying background material polarimetric signatures. The imaging approach for these measurements is reviewed, and characterizations of the system described. Finally preliminary results are shown.

Send correspondence to Jim Shell at jrshell2000@yahoo.com

2. BIDIRECTIONAL REFLECTANCE DISTRIBUTION FUNCTION

The bidirectional reflectance distribution function (BRDF) provides a complete description of the reflectance properties of a material. Specifically, BRDF quantifies the geometric distribution of radiance reflected from a surface illuminated by a source in an arbitrary position above the hemisphere of the material.

The BRDF is given by

$$f_r(\theta_i, \phi_i; \theta_r, \phi_r; \lambda) = \frac{dL_r(\theta_r, \phi_r)}{dE(\theta_i, \phi_i)} \tag{1}$$

where L_r is the surface leaving spectral radiance $\left[\frac{\mathrm{W}}{\mathrm{m}^2 \cdot \mathrm{sr} \cdot \mu\mathrm{m}}\right]$ and E is the spectral irradiance $\left[\frac{\mathrm{W}}{\mathrm{m}^2 \cdot \mu\mathrm{m}}\right]$, resulting in BRDF having units of sr^{-1}.* The incident and reflecting zenith angles are θ_i, θ_r and the corresponding azimuth angles ϕ_i, ϕ_r. The nomenclature used here is that recommended by Nicodemus,[6,7] which has subsequently been adopted by many authors.

The most general expression for BRDF fully incorporates all incident and reflected polarization states as well.[8,9] This expression may be cast as

$$\vec{L}_r(\theta_r, \phi_r) = \mathbf{F}_r(\theta_i, \phi_i; \theta_r, \phi_r; \lambda)\ \vec{E}(\theta_i, \phi_i) \tag{2}$$

where now the BRDF ($\mathbf{F}_r$) is a 4×4 Mueller matrix and the incident irradiance and surface leaving radiance are given as Stokes vectors, $\vec{E}$ and $\vec{L}_r$.

In passive, VNIR remote sensing, the polarization ellipticity may be considered negligible,[1,10] and therefore the 4×4 BRDF Mueller matrix may be reduced to a 3×3 representation. Therefore, (2) is given explicitly by

$$\begin{bmatrix} L_0 \\ L_1 \\ L_2 \end{bmatrix} = \begin{bmatrix} f_{00} & f_{01} & f_{02} \\ f_{10} & f_{11} & f_{12} \\ f_{20} & f_{21} & f_{22} \end{bmatrix} \begin{bmatrix} E_0 \\ E_1 \\ E_2 \end{bmatrix} \tag{3}$$

and the f_{00} component of $\mathbf{F}_r$ is seen to equal the scalar BRDF value, f_r of (1).

Many man-made materials, which often comprise "targets" in spectral detection algorithms, typically have spatially uniform surfaces over which the BRDF does not vary significantly (*e.g.*, painted surfaces). This results in resolved target surfaces of similar orientation having minimal pixel-to-pixel variance. Laboratory BRDF measurements successfully characterize such surfaces[11,12] and these empirical measurements are used to fit BRDF models,[13–15] enabling *a priori* predictions of spectral radiance received by a sensor given arbitrary solar and sensor orientations.

Similarly, materials comprising the "background," which are usually vegetation and soils, have been studied extensively for their anisotropic reflectance characteristics.[16] The BRDF characterization of these surfaces are used toward deducting biophysical parameters for agricultural applications or surface albedo calculations for global climate considerations.[17] The spatial extent over which these measurements are made is usually orders of magnitude greater than that of target material laboratory measurements. This is motivated in part by the relatively large Ground Separation Distance (GSD) of earth resource satellites which monitor agricultural and global climate processes.

Characterizing the BRDF of background materials at a comparable spatial extent to that of target materials is hampered by the spatial variability, or texture of natural materials. The background has significant signature variability at GSDs of interest for target detection applications. This within-material BRDF variability has been termed the bidirectional texture function[18] or the bidirectional reflectance variance function (BRVF).[19] BRVF may be considered a BRDF probability distribution function for a given GSD. As the GSD increases, the BRDF variability decreases since more of the texture is averaged within a single pixel.

The variability exhibited by background materials motivates the need for a measurement approach which captures the variability. An imaging technique has been previously reported by the authors as a suitable method,[20] and it is the polarimetric implementation of this approach which will be discussed.

*All radiometric quantities are assumed to be spectral, though not always explicitly shown.

3. GOVERNING POLARIZED RADIANCE EQUATION

Prior to discussing the polarimetric BRDF measurement approach, it is instructive to first derive an expression for the polarized radiance reaching a sensor aperture. This establishes the framework from which quantitative polarimetric remote sensing must operate, and also guides the measurement technique. The radiometric equation for the unpolarized intensity is first introduced and nomenclature established. The polarimetric representation of these equations are then derived, which results in emphasizing the role of the polarimetric BRDF. The polarized governing equation is not known to have been previously addressed in detail.

3.1. Governing Equation—Magnitude

The total radiance in the visible to near infrared (VNIR) portion of the spectrum (*i.e.* that of solar origin) reaching a sensor aperture (L_s) may be approximated as the sum of three radiance sources:

1. direct solar *reflections* from the target, L_r
2. target-reflected *downwelled* radiance from the skydome, L_d
3. *upwelled* atmosphere radiance resulting from solar scatter in the atmosphere along the target to sensor path, L_u

The order of the radiance terms above is that of typically decreasing magnitude, though the ground or target reflectance and atmospheric conditions greatly influence their relative values (*c.f.* Fig. 4.12, Tbl. 4.1 of[21]). These radiance terms are functions of the incident and reflected zenith and azimuth angles, θ_i', θ_r' and azimuth angle ϕ'.

An expression for the radiance from the direct solar reflection, L_r, is obtained by first considering the exoatmospheric solar irradiance, E_s, which propagates through the atmosphere along the solar-to-target path having a transmittance of τ_i. When incident upon a surface, it is then reflected, and again attenuated by the atmosphere along the ground-to-sensor atmospheric path by τ_r. Often the reflectance is considered Lambertian, or isotropic, such that a reflectance factor is used as an approximation to what is properly the bidirectional reflectance distribution function (BRDF), f_r. Assembling these terms, L_r may therefore be expressed as

$$L_r = \tau_r(\theta_r')\ f_r(\theta_i, \theta_r, \phi)\ \cos\theta_i'\ \tau_i(\theta_i')\ E_s(\theta_i')\ , \tag{4}$$

where the unprimed coordinate system is one relative to the normal of a material surface.

In a similar fashion, target-reflected radiance from the sky, L_d may be derived. The downwelled radiance distributed over entire hemisphere of the sky, $L_d^{\Omega_i}$, is integrated to sum irradiance contributions onto the target across the sky, which is modified by the cosine of the incident angle upon the surface normal. As before, each of these irradiance contributions is then reflected by the surface BRDF, which is then attenuated by the target-to-sensor atmospheric transmittance as before. Replacing the BRDF by an isotropic reflectance factor greatly simplifies the expression, as the reflectance factor may be placed outside the integral. However, the more stringent BRDF must be retained as it is essential to polarimetry. An appropriate expression for L_d is therefore

$$L_d = \tau_r(\theta_r')\ \iint_{\Omega_i} f_r(\theta_i, \theta_r, \phi)\ \cos\theta_i'\ L_d^{\Omega_i}(\theta_i', \phi')\ d\Omega_i'\ , \tag{5}$$

where $d\Omega_i' = \sin\theta_i'\ d\theta_i' d\phi'$.

A representation for the upwelled atmospheric radiance, L_u will not be attempted, as it is rather complex and usually approximated by atmospheric scattering codes such as MODTRAN,[22] as is the downwelled sky radiance component ($L_d^{\Omega_i}$) in equation 5. The upwelled radiance is given simply in order to show the geometry dependence as

$$L_u = L_u(\theta_r', \phi')\ . \tag{6}$$

3.2. Governing Equation—Stokes Representation

Transforming (4–6) into the polarized representation is accomplished using the Mueller-Stokes formalism commonly used in polarized radiometry. In brief, all radiometric flux values are replaced by Stokes vectors and "transfer" functions such as atmospheric transmittance and reflectance (BRDF) are replaced by Mueller matrices.

Prior to making these substitutions, some simplifications are appropriate. First, the exoatmospheric solar irradiance may be considered randomly polarized, so only the scalar magnitude (or first Stokes component) of the direct solar irradiance need be considered. Second, the atmospheric transmittance values in (4–6) all represent forward scattering, which retains the incident polarization. Therefore, the scalar values for τ_i and τ_r may be used without having to resort to a Mueller matrix representation. Equations 4–6 therefore become

$$\vec{L}_r = \tau_r(\theta_r^{'})\ \mathbf{F}_r(\theta_i, \theta_r, \phi)\ \tau_i(\theta_i^{'})\ \cos\theta_i^{'}\ E_s(\theta_i^{'}) \tag{7}$$

$$\vec{L}_d = \tau_r(\theta_r^{'}) \iint_{\Omega_i} \mathbf{F}_r(\theta_i, \theta_r, \phi)\ \cos\theta_i^{'}\ \vec{L}_d^{\Omega_i}(\theta_i^{'}, \phi_i^{'})\ d\Omega_i^{'} \tag{8}$$

$$\vec{L}_u = \vec{L}_u(\theta_r^{'}, \phi_r^{'}) \tag{9}$$

where $\mathbf{F}_r$ is now the polarimetric BRDF (pBRDF). Some knowledge of the upwelled polarized radiance ($\vec{L}_u$) along the target and sensor may be gained from Rayleigh scattering theory and other sources such as Coulson[23] and Chandrasekhar.[24] However, knowledge of the polarized downwelled radiance, $\vec{L}_d^{\Omega_i}$ is more problematic since this term often has a high spatial variability, *e.g.*, varying cloud cover.

The total polarized radiance reaching a sensor aperture is then

$$\vec{L}_s = \vec{L}_r + \vec{L}_d + \vec{L}_u\ . \tag{10}$$

Atmospheric scattering, generally proportional to λ^{-4}, results in $\vec{L}_d$ and $\vec{L}_u$ having relatively large magnitudes at shorter wavelengths compared to $\vec{L}_r$, especially from orbital altitudes. Atmospheric polarimetric remote sensing uses this phenomena to minimize ground reflected polarization signatures to better extract atmospheric water vapor and aerosol properties.[25]

Similarly, for polarimetric remote sensing of land features one wants the magnitude of the direct solar reflected radiance to be large compared to the reflected radiance from the downwelled sky and upwelled atmospheric scattering, *i.e.*, $\vec{L}_r > \vec{L}_d, \vec{L}_u$. This provides optimal conditions for estimating the polarimetric BRDF, $\mathbf{F}_r$. Exploiting polarimetric signatures in a manner analogous to spectral signatures requires estimating $\mathbf{F}_r$ given the polarized radiance reaching the aperture, $\vec{L}_s$.

Estimating $\mathbf{F}_r$ given the radiance at the sensor aperture proceeds as

$$\vec{L}_r = \vec{L}_s - \vec{L}_d - \vec{L}_u \tag{11}$$

$$\tau_r\ \mathbf{F}_r\ \tau_i\ \cos\theta_i^{'}\ E_s = \vec{L}_s - \tau_r \iint_{\Omega_i} \mathbf{F}_r\ \cos\theta_i^{'}\ \vec{L}_d^{\Omega_i}\ d\Omega_i^{'} - \vec{L}_u\ . \tag{12}$$

Since the exoatmospheric irradiance is randomly polarized, only the first column of the pBRDF Mueller matrix is of concern in the $\vec{L}_r$ expression. In fact, overhead polarimetric remote sensing may only retrieve the first column of the polarimetric BRDF matrix. (Solving for other matrix elements requires illumination by varying polarization states). With this consideration (12) may be expressed as

$$\tau_r \begin{bmatrix} f_{00} \\ f_{10} \\ f_{20} \end{bmatrix} \tau_i\ \cos\theta_i^{'}\ E_s = \vec{L}_s - \tau_r \iint_{\Omega_i} \mathbf{F}_r\ \cos\theta_i^{'}\ \vec{L}_d^{\Omega_i}\ d\Omega_i^{'} - \vec{L}_u \tag{13}$$

with the first column of the pBRDF given by

$$\begin{bmatrix} f_{00} \\ f_{10} \\ f_{20} \end{bmatrix} = \frac{\vec{L}_s - \tau_r \iint_{\Omega_i} \mathbf{F}_r\ \cos\theta_i^{'}\ \vec{L}_d^{\Omega_i}\ d\Omega_i^{'} - \vec{L}_u}{\tau_r\ \tau_i\ \cos\theta_i^{'}\ E_s}\ . \tag{14}$$

Solving for $\mathbf{F}_r$ is complicated by its inclusion in the integral of the $\vec{L}_d$ term, which also contains the highly spatially variable and generally unknown downwelled radiance component, $\vec{L}_d^{\Omega_i}$. However, under nominal sky conditions, the magnitude of the direct solar irradiance for $\lambda > 600$ nm is five times that of the integrated sky-dome irradiance, increasing to 10x for $\lambda > 1000$ nm. This makes it reasonable to approximate the polarized radiance contribution of the downwelled sky radiance as an error term.

$$\begin{bmatrix} f_{00} \\ f_{10} \\ f_{20} \end{bmatrix} = \frac{\vec{L}_s - \vec{L}_u}{\tau_r \, \tau_i \, \cos\theta_i' \, E_s} - \frac{\tau_r \iint_{\Omega_i} \mathbf{F}_r \, \cos\theta_i' \, \vec{L}_d^{\Omega_i} \, d\Omega_i'}{\tau_r \, \tau_i \, \cos\theta_i' \, E_s} \tag{15}$$

$$= \frac{\vec{L}_s - \vec{L}_u}{\tau_r \, \tau_i \, \cos\theta_i' \, E_s} - \begin{bmatrix} \epsilon_0 \\ \epsilon_1 \\ \epsilon_2 \end{bmatrix} . \tag{16}$$

Therefore, polarimetric remote sensing may recover the first column of polarimetric BRDF Mueller matrix to within the error resulting from downwelled sky radiance, presented as

$$\begin{bmatrix} f_{00} + \epsilon_0 \\ f_{10} + \epsilon_1 \\ f_{20} + \epsilon_2 \end{bmatrix} = \frac{\vec{L}_s - \vec{L}_u}{\tau_r \, \tau_i \, \cos\theta_i' \, E_s} . \tag{17}$$

Note that ϵ_0 is always positive, and for diffuse surfaces the ratio of $\frac{\epsilon_0}{f_{00}}$ is equivalent to the ratio of the downwelled sky irradiance to the direct solar irradiance. The linear polarization terms ϵ_1 and ϵ_2 may either be positive or negative and represent the influence of the partially polarized downwelled sky radiance.

4. POLARIMETRIC BRDF MEASUREMENT APPROACH

Ideally, BRDF measurements are made in a lab environment using a "point" illumination source with careful control and minimization of stray light. However, many materials such as vegetation do not lend themselves to easy indoor measurements due to alteration of their natural state or simply from their physical size (*e.g.*, a tree canopy). Outdoor BRDF measurements of such materials becomes a necessity, and many approaches have been successfully employed.[26–29] Wide field of view (FOV) imaging systems may be used which efficiently enable the simultaneous measurement of multiple scattering angles.[30–32]

Our approach is having a narrow FOV ($\approx 10°$) imaging system to make BRDF measurements. Each image pixel is approximated as the same scattering angle as that at the center of the image, such that the average radiance across the focal plane enables determination of the BRDF. Such an approach limits the scattering angle resolution to the FOV, but this is not a concern for most natural surfaces which are not appreciably specular and hence do not have rapid BRDF changes over the 10° FOV of the system. The impetus for this technique is the ability to quantify the the BRDF variability (as discussed in §2). Multiple scattering angles are sampled by repositioning the camera in the hemisphere above the measurement surface.

This technique may be used at any distance from the measurement surface—the only prerequisite is that the ground FOV (GFOV) is large enough that it adequately integrates the spatial variability or texture of the material. For instance, a GFOV of 1 foot may be adequate for grass, asphalt and aggregate; but measurements of tree canopies and shrubs would require a larger GFOV. For easy field use not requiring elevated platforms or other positioning devices, an operating distance for the measurements discussed here was 6 feet, providing a GFOV of approximately 1 foot.

4.1. BRDF Measurement

A successful technique for outdoor BRDF measurements may be developed by considering the radiance contributions to a sensor (*c.f.* equation (10)). It is first noted that imaging surfaces at a distance of 6 feet results in negligible atmospheric scattering along the surface to sensor path, such that $\vec{L}_u \approx 0$. The surface radiance is therefore composed of the direct solar and downwelled sky reflectance, or $\vec{L}_r$ and $\vec{L}_d$. The measurement made when the surface is illuminated by the sun and downwelled sky radiance will be referred to as image C (Figure 2).

The downwelled sky radiance is a stray light source for the purpose of BRDF measurements. It may be directly measured and eliminated via an image subtraction technique. $\vec{L}_d$ is measured by placing the measurement area in shadow, and imaging the shadowed surface (image D). In this manner it is seen that

$$\vec{L}_r \propto \mathtt{C} - \mathtt{D} \;=\; (\vec{L}_r + \vec{L}_d) - (\vec{L}_d)\;. \tag{18}$$

The error terms shown in equation (17) are therefore eliminated by the "shadow" image. This is quite valuable, as comparison of the C and $\mathtt{C}-\mathtt{D}$ data quantifies the change to the linear Stokes components resulting from the sky polarization.

4.2. Radiance Calibration

The "digital counts" recorded by the imaging system may be transformed into absolute radiance levels by use of a Spectralon calibration target. Spectralon has a highly Lambertian, angular-invariant BRDF of $\frac{\rho}{\pi}$, with a randomly polarized reflectance of $\rho \geq 0.97$ across most of the VNIR spectrum.[33] As with the surface being measured, images of the calibration target are taken both in sun and in shadow, images A and B, respectively.

When acquiring multiple images over a short time period such that the atmospheric conditions and solar zenith position (θ_i) do not change appreciably, the BRDF may be determined by the ratio of the known calibration target BRDF to that of the unknown surface or

$$\frac{L_r^{cal}}{L_r^{sur}} = \frac{\frac{\rho}{\pi}}{f_r} \longrightarrow f_r = \frac{\rho}{\pi}\frac{L_r^{sur}}{L_r^{cal}}\;. \tag{19}$$

In terms of the digital counts of the pixels in each of the four images, A through D, the BRDF is

$$f_r = \frac{\rho}{\pi}\left[\frac{\mathtt{C}-\mathtt{D}}{\mathtt{A}-\mathtt{B}}\right]\;. \tag{20}$$

When imaging a calibration target such that it occupies the full FOV, this technique also self-corrects for the so called "lens falloff" irradiance reduction away from the center of the focal plane.

4.3. Polarimetric BRDF

The polarized radiance leaving the surface may be quantified as a Stokes vector using well-established approaches.[8,34] In our implementation, images of the surface are acquired under four different linear polarization filter orientations relative to the horizon: 0°, 45°, 90° and 135°. This enables derivation of the Stokes vector according to

$$\begin{bmatrix} S_0 \\ S_1 \\ S_2 \end{bmatrix} = \begin{bmatrix} \frac{I_0+I_{90}+I_{45}+I_{135}}{2} \\ I_0 - I_{90} \\ I_{45} - I_{135} \end{bmatrix} \tag{21}$$

where $I_{\mathtt{xx}}$ represents an image acquired with the polarization filter set at xx°. It is noted that the first Stokes component is derived using an average of both sets of cross-polarized images.

In terms of the images using the calibration target, it is seen from equations (20, 21) that the polarimetric BRDF is therefore

$$\begin{bmatrix} f_{00} \\ f_{10} \\ f_{20} \end{bmatrix} = \frac{\rho}{\pi(\mathtt{A}_{\mathtt{arb}} - \mathtt{B}_{\mathtt{arb}})} \begin{bmatrix} \frac{1}{2}\left[(\mathtt{C}_0 - \mathtt{D}_0) + (\mathtt{C}_{90} - \mathtt{D}_{90}) + (\mathtt{C}_{45} - \mathtt{D}_{45}) + (\mathtt{C}_{135} - \mathtt{D}_{135})\right] \\ (\mathtt{C}_0 - \mathtt{D}_0) - (\mathtt{C}_{90} - \mathtt{D}_{90}) \\ (\mathtt{C}_{45} - \mathtt{D}_{45}) - (\mathtt{C}_{135} - \mathtt{D}_{135}) \end{bmatrix}\;, \tag{22}$$

where arb indicates an arbitrary polarization filter orientation for imaging the calibration target, since this radiance is randomly polarized.

To summarize, for each hemispherical scattering position, a total of 8 images are acquired of the target surface, 4 polarization orientations with 2 illumination conditions (full sun and shadow). A minimum of 2 calibration target images must be taken, one for each illumination condition. Therefore a data set at one scattering position comprises 10 images.

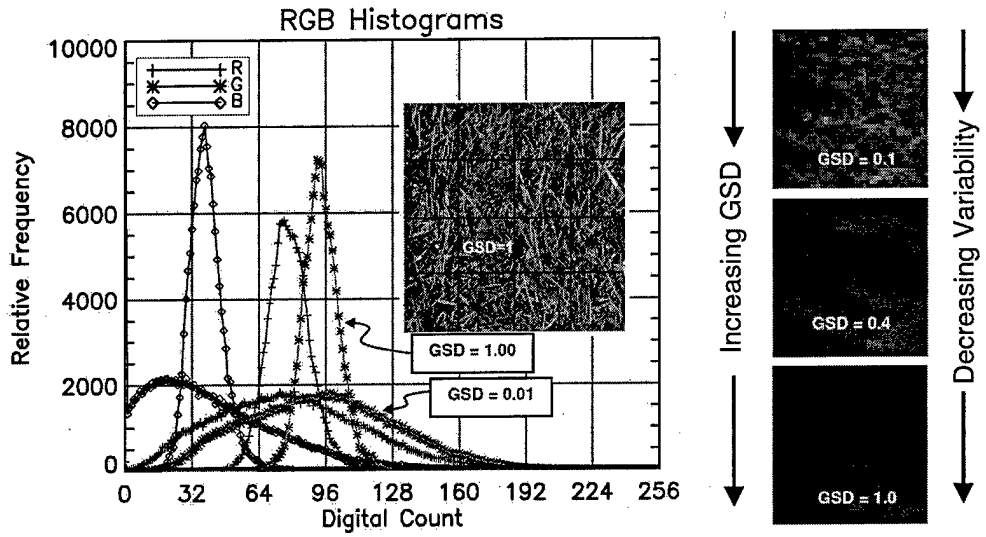

Figure 1. The RGB BRDF distributions or BRFV for a "grass" measurement. Histograms are shown for the full image resolution and at an arbitrarily defined "GSD = 1". The averaging of the texture as a function of GSD is illustrated at right.

4.4. BRDF Probability Distribution (BRVF) Calculation

Thus far, only the average digital count values over the entire image have been considered in deriving the BRDF. However, the impetus for this technique is the ability to quantify the BRDF variability, or BRVF discussed in §2. The variability is obviously a function of the GSD, as a larger GSD results in greater averaging of texture within a pixel, and hence decreased pixel to pixel variability.

The high-resolution images acquired with the BRDF measurement system may then be used to generate the BRVF given the anticipated GSD of a remote sensing sensor. Generating the BRVF is accomplished by convolving the image, $f[x, y]$, with a convolution kernel $h[x, y]$ representative of the GSD of interest. The result is a low-pass filtered image, $g[x, y]$ with the spatial texture representative of the GSD of $h[x, y]$. This is presented mathematically as

$$g[x, y] = \frac{1}{X^2} \sum_{i=0}^{m-1} \sum_{j=0}^{n-1} f[x, y]\ h[x - i, y - j] \tag{23}$$

where X^2 is a weighting factor such that the average magnitude of $g[x, y]$ is that of the original image, $f[x, y]$. Ideally $h[x, y]$ is the point spread function of the remote sensing platform in question, but for quick processing a simple function with a unit magnitude and square spatial extent is used (termed a RECT function by some[35]). Figure 1 illustrates the effect using a simple color (RGB) image of "grass" taken with a commercial digital camera.

Unlike the polarimetric BRDF determination, the accuracy of the BRVF depends upon the degree of the spatial registration of the four sets of polarized C and D images. When the size of the convolution kernel is commensurate with the spatial registration accuracy, significant errors result. The same is true of movement of measurement surface while acquiring the four polarization orientations, *e.g.* grass blowing in the wind. As required, the C and D image sets should be spatially registered prior to performing BRVF calculations.

A summary of the general measurement steps for this technique is presented as Figure 2. Depending on the polarimetric imaging system used to make the measurements, this process should be modified accordingly, such as spectral filter changes, etc.

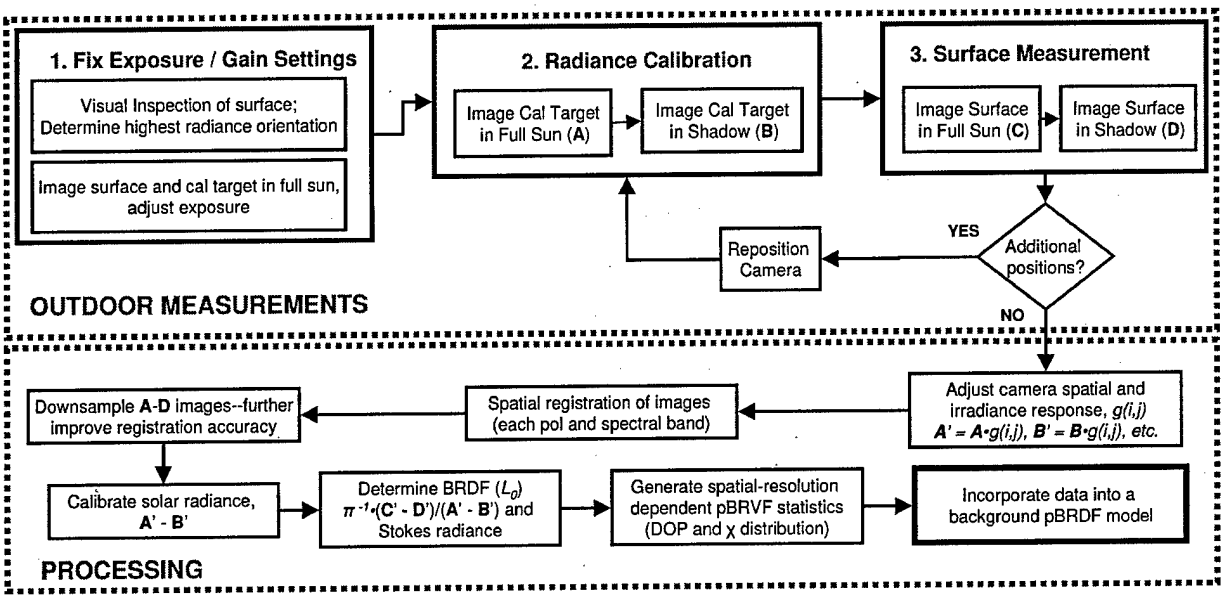

Figure 2. Measurement and process flow for making polarimetric BRDF and BRVF measurements with the camera system.

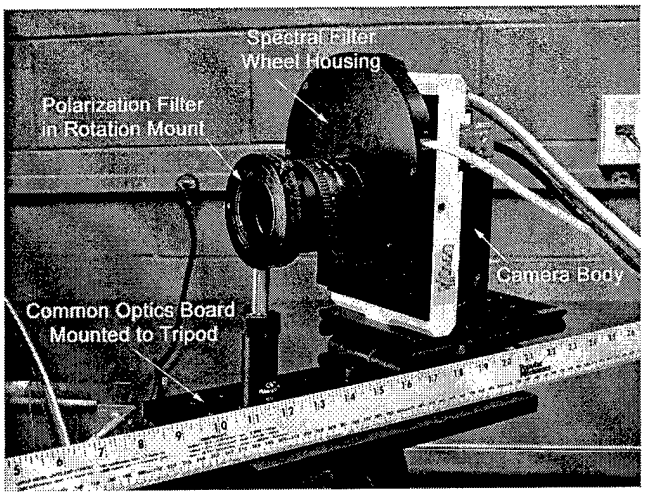

Figure 3. The assembled imaging system mounted on a tripod.

5. IMAGING SYSTEM DESCRIPTION & CHARACTERIZATION

The imaging system consists of a SenSys 1602E camera having a 1536×1024 thermoelectric-cooled, 12-bit silicon CCD with a response nonlinearity $\leq 0.5\%$. A filter wheel located between the lens and the CCD is used to mount 25 mm diameter band-pass filters. The spectral filter wheel housing accepts a standard F-mount lens, to which a Nikon 50 mm, f/1.8 lens is used. A linear polarization filter is mounted external to the lens on an optics post in a precision rotary mount, which is mounted to a common optics board with the camera. This assembly is then mounted on a tripod. To demonstrate the technique, data is only taken at two spectral bands, 550 ± 5 nm and 750 ± 12 nm. An overview of the system is shown in Figure 3.

The imaging system was characterized in order to gain an understanding of the measurement uncertainties

and limitations. First, it was noted the "dark" images of the camera were highly repeatable, and have negligible error contribution to the series of images used to make a measurements.

The lens falloff, or focal plane irradiance decrease away from the center of the array, was also quantified by imaging into an integrating sphere, which provided a uniform radiance field. At an aperture setting of f/8.0, where the system is usually operated, the edge of the measurement area on the focal plane has a response of 0.94 ± 0.01 relative to that at the center of the array. Correction to the lens falloff is only necessary under circumstances when the calibration target may not be imaged over the full FOV of the system.

5.1. Polarization Filter Alignment Errors

A thorough error analysis of the polarization errors is quite involved and beyond the scope of this paper. Only the final error equations, in terms of the Stokes components, and the anticipated net error are presented. First, there is uncertainty in the polarization filter orientation relative to the local horizon, which is considered the absolute reference frame for the polarization orientation. This error is not as critical, as it does not impact the measured DOP, but only the relative magnitude between the S_1 and S_2 Stokes components.

More important are the errors resulting from manually positioning the polarization filter in the four orientations. This error is complex and is a function of the incident polarization magnitude and direction, and of course the polarization filter orientation error, $\epsilon_{\mathtt{xx}}$ for the $\mathtt{xx}^\circ$ filter position. It may be shown that the error in the derived intensity or first Stokes component is given by

$$\begin{aligned} S_0 = S_{0_{in}} + \epsilon_{0_{tot}} = S_{0_{in}} &+ \frac{S_{1_{in}}}{4}\Big\{[\cos(2\epsilon_0) - \cos(2\epsilon_{90})] + [\sin(2\epsilon_{135}) - \sin(2\epsilon_{45})]\Big\} \\ &+ \frac{S_{2_{in}}}{4}\Big\{[\cos(2\epsilon_{45}) - \cos(2\epsilon_{135})] + [\sin(2\epsilon_0) - \sin(2\epsilon_{90})]\Big\} \end{aligned} \tag{24}$$

with errors in the linear Stokes components given by

$$S_1 = S_{1_{in}} + \epsilon_{1_{tot}} = \frac{1}{2}\Big\{S_{1_{in}}\left[\cos(2\epsilon_0) + \cos(2\epsilon_{90})\right] + S_{2_{in}}\left[\sin(2\epsilon_0) + \sin(2\epsilon_{90})\right]\Big\} \tag{25}$$

$$S_2 = S_{2_{in}} \pm \epsilon_{2_{tot}} = \frac{1}{2}\Big\{S_{2_{in}}\left[\cos(2\epsilon_{45}) + \cos(2\epsilon_{135})\right] - S_{1_{in}}\left[\sin(2\epsilon_{45}) + \sin(2\epsilon_{135})\right]\Big\}\,. \tag{26}$$

It is estimated that the positioning accuracy of the polarization filters is $\epsilon_{xx} = 0 \pm 0.25^\circ$ at a 2σ confidence level. Numerical simulations of equations (24)–(26) result in an anticipated 2σ error less than $\pm 1.2\%$ for all Stokes component.

5.2. Finite Filter Contrast Error

Next, the error resulting from the finite contrast or cross polarized "leakage" are presented. This performance metric may be given by the cross-polarized transmittance relative to the like-polarized transmittance, $\tau_\otimes$. This error produces the intuitive result of overestimating the total intensity, S_0, and underestimating the linear Stokes components. Again without derivation, this results in

$$S_0 = (1 + \tau_\otimes)S_{0_{in}}, \quad S_1 = (1 - \tau_\otimes)S_{1_{in}} \text{ and } \quad S_2 = (1 - \tau_\otimes)S_{2_{in}}, \tag{27}$$

with the impact on DOP given by

$$DOP = \left(\frac{1 - \tau_\otimes}{1 + \tau_\otimes}\right) DOP_{in}\,. \tag{28}$$

It is noted that this error is systematic and may be corrected with knowledge of $\tau_\otimes$. For our system, $\tau_\otimes$ at 550 nm is estimated as 0.015.

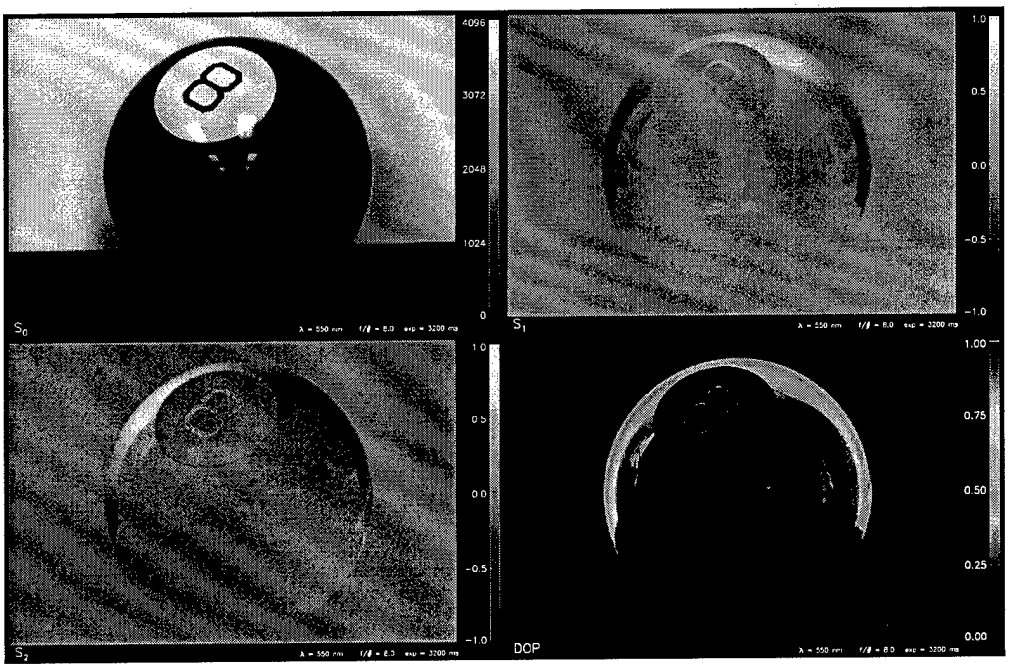

Figure 4. The Stokes and DOP images of a "Magic 8-ball" under ambient lighting conditions at 550 nm. S_0 (*top left*), S_1 (*top right*), S_2 (*bottom left*) and DOP (*bottom right*).

5.3. Test Image

Having gained an understanding of the system performance, a data set was acquired by imaging a "Magic 8-ball." The ball is well-suited for demonstrating polarization phenomenology as it has a highly smooth, specular surface, including regions of black and white having very low and very high diffuse (randomly polarized) reflectance. In addition, the curvature of the ball provides multiple specular view angles. The ball was imaged under ambient lighting conditions in front of a Spectralon panel. The images were processed according to equation (21) providing the Stokes vectors, from which the DOP was calculated (Figure 4). The DOP image provides a pleasing result—reflectance from the Spectralon panel off the edges of the ball provide a DOP commensurate with that expected from Fresnel reflectance, with a peak magnitude reached near Brewster's angle.

6. PRELIMINARY RESULTS

I plan on including some lab measurements of "gravel" to demonstrate the anticipated outdoor results. These indoor measurements will admittedly be approximations, due to the lack of a uniform irradiance source. Will include a figure similar to the "8-ball" one, and also generate BRVF statistics.

7. CONCLUSIONS

The polarimetric governing equation for reflected radiance has been developed and shown to provide a quantitative framework from which polarimetric remote sensing must operate. Measuring background material polarization signatures quantifies the noise floor for polarimetric target detection and identification algorithms. The presented measurement technique enables polarized signatures tailored to the point spread function or GSD of specific imaging systems. Such measurements may be applied to polarimetric BRDF models, enabling radiometrically-accurate synthetic image generation. Synthetic hyperspectral polarimetric imagery allows extensive modelling of the varying conditions under which spectral and/or polarimetric target detection and identification algorithms may operate.

DISCLAIMER

The views expressed in this article are those of the authors and do not reflect the official policy or position of the U. S. Air Force, Department of Defense, or the U. S. Government.

REFERENCES

1. R. Walraven, "Polarization imagery," in *Optical Polarimetry: Instrumentation and Applications*, R. M. A. Azzam and D. L. Coffeen, eds., *Proc. SPIE* **112**, pp. 164–167, 1977.
2. W. G. Egan, "Optical Stokes parameters for farm crop identification," *Remote Sensing of Env* **1**, pp. 165–180, 1970.
3. *Remote Sensing in Polarized Light, NASA Conference Publication* **3014**, 1987.
4. W. G. Egan, *Optical Remote Sensing Science and Technology*, Marcel Dekker, Inc., 2004.
5. R. Mayer, R. Priest, C. Steliman, G. Hazel, and A. Schaum, "Detection of camouflaged targets in cluttered backgrounds using fusion of near simultaneous spectral and polarimetric imaging," tech. rep., Naval Research Lab, Washington DC Optical Sciences Division, August 2000. Approved for Public Release.
6. F. E. Nicodemus, "Reflectance nomenclature and directional reflectance and emissivity," *Applied Optics* **9**, pp. 1474–1475, June 1970.
7. F. E. Nicodemus, J. C. Richmond, *et al.*, "Geometrical considerations and nomenclature for reflectance; NBS Monograph 160," tech. rep., Department of Commerce, National Bureau of Standards, 1977.
8. W. S. Bicket and W. M. Bailey, "Stokes vectors, Mueller matrices, and polarized scattered light," *Americal Journal of Physics* **53**, pp. 468–478, May 1985.
9. D. S. Flynn and C. Alexander, "Polarized surface scattering expressed in terms of a bidirectional reflectance distribution function matrix," *Optical Engineering* **34**, pp. 1646–1650, 1995.
10. K. L. Coulson, *Polarization and Intensity of Light in the Atmosphere*, A. DEEPAK Publishing, 1988.
11. D. H. Goldstein, "Polarimetric characterization of federal standard paints," in *Polarization Analysis, Measurement, and Remote Sensing III, Proc. SPIE* **4133**, pp. 112–123, 2000.
12. M. P. Fetrow, S. H. Sposato, K. P. Bishop, and T. R. Caudill, "Spectral polarization signatures of materials in the LWIR," in *Polarization Analysis, Measurement, and Remote Sensing III, Proc. SPIE* **4133**, pp. 249–260, 2000.
13. K. E. Torrance and E. M. Sparrow, "Theory for off-specular reflection from roughened surfaces," *Journal of the Optical Society of America* **57**, pp. 1105–1114, September 1967.
14. J. R. Maxwell, J. Beard, S. Weiner, D. Ladd, and S. Ladd, "Bidirectional reflectance model validation and utilization," Tech. Rep. AFAL-TR-73-303, Environmental Research Institute of Michigan (ERIM), October 1973.
15. R. G. Priest and S. R. Meier, "Polarimetric microfacet scattering theory with applications to absorptive and reflective surfaces," *Optical Engineering* **41**, pp. 988–993, May 2002.
16. M. von Schönermark, B. Geiger, and H. P. Röser, *Reflection Properties of Vegetation and Soil with a BRDF Database*, Wissenschaft and Technik Verlag, Berlin, 2004.
17. *Remote Sensing Reviews*, **18**, 2000. Special issue on multi-angle remote sensing.
18. K. J. Dana, B. van Ginneken, S. K. Nayar, and J. J. Koenderink, "Reflectance and texture of real-world surfaces," *ACM Transactions on Graphics (TOG)* **18**, pp. 1–34, January 1999.
19. W. Ni, C. E. Woodcock, and D. L. B. Jupp, "Variance in bidirectional reflectance over discontinuous plant canopies," *Remote Sensing of Environment* **69**, pp. 1–15, July 1999.
20. J. R. Shell, C. Salvaggio, and J. R. Schott, "A novel BRDF measurement technique with spatial resolution-dependent spectral variance," in *IEEE International Geoscience and Remote Sensing Symp.*, pp. 4754–4757, Sept 2004.
21. J. R. Schott, *Remote Sensing: The Image Chain Approach*, Oxford University Press, 1997.
22. A. Berk, T. W. Cooley, G. P. Anderson, *et al.*, "MODTRAN5: a reformulated atmospheric band model with auxiliary species and practical multiple scattering options," in *Remote Sensing of Clouds and the Atmosphere IX*, A. Comeron, M. R. Carleer, R. H. Picard, and N. I. Sifakis, eds., *Proc. SPIE* **5571**, pp. 78–85, November 2004.
23. K. L. Coulson, J. V. Dave, and Z. Sekera, *Tables Related to Radiation Emerging from a Planetary Atmosphere with Rayleigh Scattering*, University of California Press, Berkeley, CA, 1960.
24. S. Chandrasekhar, *Radiative Transfer*, Clarendon Press, Oxford, 1950.
25. M. Leroy, J. L. Deuzé, F. M. Bréon, *et al.*, "Retrieval of atmospheric properties and surface bidirectional reflectances over the land from POLDER (processing algorithms)," *J. of Geophysical Res.* **102**, pp. 17023–17037, July 27 1997.
26. D. W. Deering and P. Leone, "A sphere-scanning radiometer for rapid directional measurements of sky and ground radiance," *Remote Sensing of Environment* **19**, pp. 1–24, February 1986.
27. C. Walthall, J.-L. Roujean, and J. Morisette, "Field and landscape BRDF optical wavelength measurements: Experience, techniques and the future," *Remote Sensing Reviews* **18**, pp. 503–531, 2000.
28. S. R. Sandmeier and K. I. Itten, "A field goniometer system (FIGOS) for acquisition of hyperspectral BRDF data," *IEEE Transactions on Geoscience and Remote Sensing* **37**, pp. 978–986, March 1999.
29. S. R. Sandmeier, "Acquisition of bidirectional reflectance factor data with field goniometers," *Remote Sensing of Environment* **73**, pp. 257–269, September 2000.

30. J. S. Czapla-Myers, K. J. Thome, and S. F. Biggar, "Optical sensor package for multiangle measurements of surface reflectance," in *Imaging Spectrometry VII*, M. R. Descour and S. S. Shen, eds., *Proc. SPIE* **4480**, pp. 326–333, 2002.
31. J. Y. Han and K. Perlin, "Measuring bidirectional texture reflectance with a kaleidoscope," *ACM Transactions on Graphics (TOG)* **22**, pp. 741–748, July 2003.
32. K. J. Dana and J. Wang, "Device for convenient measurement of spatially varying bidirectional reflectance," *JOSA A* **21**, pp. 1–12, January 2004.
33. D. H. Goldstein, "Polarimetric characterization of spectralon," in *Polarization: Measurement, Analysis, and Remote Sensing II, Proc. SPIE* **3754**, pp. 126–136, 1999.
34. R. A. Chipman, *Handbook of Optics*, vol. II, ch. 22. Optical Society of America, second ed., 2000.
35. J. D. Gaskill, *Linear Systems, Fourier Transformas, and Optics*, John Wiley and Sons, 1978.